Stoch Environ Res Risk Assess (2012) 26:545–556
DOI 10.1007/s00477-011-0520-6

ORIGINAL PAPER

Numerical and multivariate stochastic approaches to characterize flow in a constructed wetland basin

Xiaohua Wei · Anand K. Plappally · Alfred B. O. Soboyejo · Bin Dong · Zhi Mao · Larry C. Brown

Published online: 14 September 2011

Abstract Reduction in specific and viscous dissipation rate in surface waters by flow control and contaminant removal are the goals of constructed wetlands. A two-dimensional simulation study on surface flow through a constructed wetland in Guilin, China is performed. The flow through the wetland is modeled and dynamically simulated by distinct case studies by varying both inlet width and inflow rate. Nonlinear increase in peak dynamic pressure and specific dissipation rates as a function of increasing inflow rate is reported for the different cases studied. The results of the numerical models confirm an increase in viscous dissipation, shear stress and dynamic pressure within the wetland with increase in inflow rate. These modeling results are used as inputs for performing a statistical data analysis. Further, a multivariate stochastic statistical framework has been proposed for the prediction of dissipation as a function of variables including inflow rate, inlet geometry and wall shear stress. Multivariate and variance analysis is performed to validate the appropriateness of the theoretical models proposed. Results provide simplified meaningful suggestions to constructed wetland design and related applications.

Keywords Constructed wetland · Flow dynamics · Two-dimensional · Numerical simulation · Stochastic analysis · Multivariate

X. Wei (✉) · A. K. Plappally · A. B. O. Soboyejo · L. C. Brown
Department of Food, Agricultural and Biological Engineering, The Ohio State University, Columbus, OH 43210-1058, USA
e-mail: xhwei.1119@gmail.com

B. Dong · Z. Mao
State Key Laboratory of Water Resources and Hydropower Engineering Science, Wuhan University, Wuhan 430072, China

List of symbols

WRSIS	Wetland Reservoir-Subirrigation-System
FCWS	Farmland-Channel-Wetland-System
NSRA	Navier–Stokes equations with Reynolds Averaging
W	Inlet width
q	Mass inflow rate
k	Turbulent kinetic energy
Re	Reynolds number
t	Time
v_x	Velocity in x direction
v_y	Velocity in y direction
v	Kinematic viscosity
τ_{ij}	Critical bed-shear stress on wall
v	Velocity magnitude
p	Dynamic pressure
ω	Specific dissipation rate
τ	Wall shear stress
$E(v)$	Maximum velocity
$E(p)$	Maximum dynamic pressure
$E(\omega)$	Peak dissipation rate
$E(\tau)$	Peak wall shear stress
R^2	Coefficient of determination
S	Sample standard deviation
σ	Standard deviation
μ	Mean deviation
D_n	Maximum discrepancy
$\rho_{x_{i,j}}$	Correlation coefficient
$\lambda_{i,j}$	Eigenvalue

1 Introduction

Wetlands help to treat polluted water by removing contaminants such as chemicals, pesticides, sediment and

fertilizers through natural physical and biochemical processes (Mitsch and Wise 1998; Kadlec 1999; Knight et al. 2000) Building upon this knowledge, a Wetland Reservoir Subirrigation System (WRSIS) was developed in Ohio, USA (Allred et al. 2001), which is comprised of a constructed wetland and a water storage reservoir linked to a network of subsurface drainage pipes used at different times to either drain or irrigate crops through the root zone (Fig. 1). Runoff and subsurface drainage are collected in the constructed wetland. Natural processes allow the wetland to partially treat the water through removal of nutrients, pesticides, and sediment. The water is then routed to a storage reservoir and held until needed to subirrigate crops during the growing season. Weir-type hydraulic control structures are manually operated to regulate the surface water levels in the wetland and shallow ground water levels in soil, while limiting offsite discharge. WRSIS operates in a closed loop mode for the most part, and very little water is released outside the system. Allred et al. (2001, 2003, 2007) and others have assessed benefits from this system, including: (1) greater crop yields, (2) additional wetland habitat, and (3) reductions in the amount of nutrients, pesticides, and sediment discharged into local waterways. These types of systems can play an effective role in reducing pollutant loss from farmland, improving irrigation water supply and increasing grain output. In China, irrigation and drainage systems are mostly open channel for rice-based irrigation schemes.

The relatively high expenditure for subsurface drainage is a major limitation for implementation of the typical Ohio, USA WRSIS concept, especially in southern China. Therefore, a similar system named Farmland-Channel-Wetland-System (FCWS) was introduced as an adaptation of the Ohio WRSIS in Guilin, China (Wei et al. 2007; Shan et al. 2008). This new system is suitable for irrigation schemes with open channels (Fig. 2), and is composed by two parts: Farmland and constructed wetlands, which are linked by open channels. Farmland drainage flows into the wetland system, and after natural water treatment occurs,

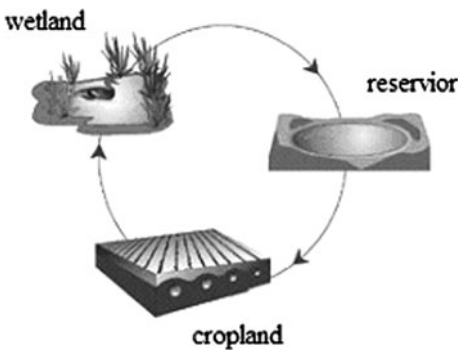

Fig. 1 Composition of the WRSIS concept in Ohio

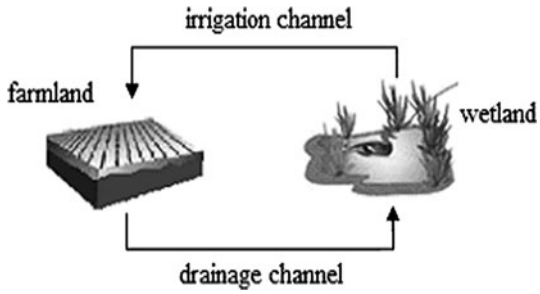

Fig. 2 Composition of the FCWS in Guilin, China

the water can be reused for irrigation or can be dispersed into a drainage channel or river.

Among a large number of articles devoted to the investigation of flow characteristics in water bodies involving the Navier–Stokes equation, there is a relatively small amount of literature with stochastic multi-parameter approaches appended to computational flow modeling (Davies et al. 2003). Simulation on the Monash University Research Wetland was conducted by Somes et al. (1999) using MIKE 21, a two-dimensional model developed by Somes et al. at the Danish Hydraulic Institute. Hydraulic roughness, water depth and vegetation contents were found to be the factors that controlled flow within the wetland. They found that eddy viscosity was the key parameter by which the flow forces within the wetland were inertial rather than frictional. Wetlands are ecosystems that are highly effective in dissipation of energy (Pokorny et al. 2010). These ecosystems include plant cover or vegetation. This emergent vegetation and its effects on wetland hydraulics were also studied by Bernhard et al. (2004), and more than 13 pond shapes and their flow characteristics as a function of inlet and outlet location, basin morphology were studied by Persson et al. (1999).

Hydrodynamic analysis of wetlands is complicated by the large variation in shapes, vegetation, seepage, inflow rate, influent flow chemistry, etc. Following this, a study is undertaken to understand the variability in constructed wetland flow dynamics as a function of inlet width and inflow rate. This variability suggests that a statistical framework is required for improved quantification and modeling flow dynamics which help in water treatment and management.

1.1 Site description

In Guilin, the FCWS was introduced as illustrated in a rice-based irrigation scheme in Fig. 3. Herein drainage and surface water from the paddy fields are routed to a constructed wetland via a drainage channel, instead of directly to a drainage ditch. The harvested drainage water once treated in the constructed wetland is routed to a main

drainage canal within the drainage and irrigation network. One paddy field was transformed into the constructed wetland (Fig. 3) and treats the nutrients from upper paddy field drainage (Shan et al. 2008).

In flow experiments performed at the Guilin site (Shan et al. 2008), the farmland area is divided into three separate zones by the two irrigation and drainage double-duty channels coming from Qingshitan Reservoir. The study region for FCWS is the paddy field area between the two channels and consists of 15 paddy fields with a total area of about 0.8 ha. Drainage from these 14 paddy fields drain to the constructed wetland (0.04 ha).The drainage area to constructed wetland area ratio is 20:1. The maximum depth of the constructed wetland is 60 cm while the maximum water depth is 40 cm. Two islands were constructed in the middle of the basin to guide inflow and improve residence time.

1.2 Numerical methods and flow models

A numerical model mesh for the two-dimensional study was developed as illustrated in Fig. 4 using Gambit, and plotted in Tecplot 360 (Fluent 6.3 2006; Tecplot Inc.

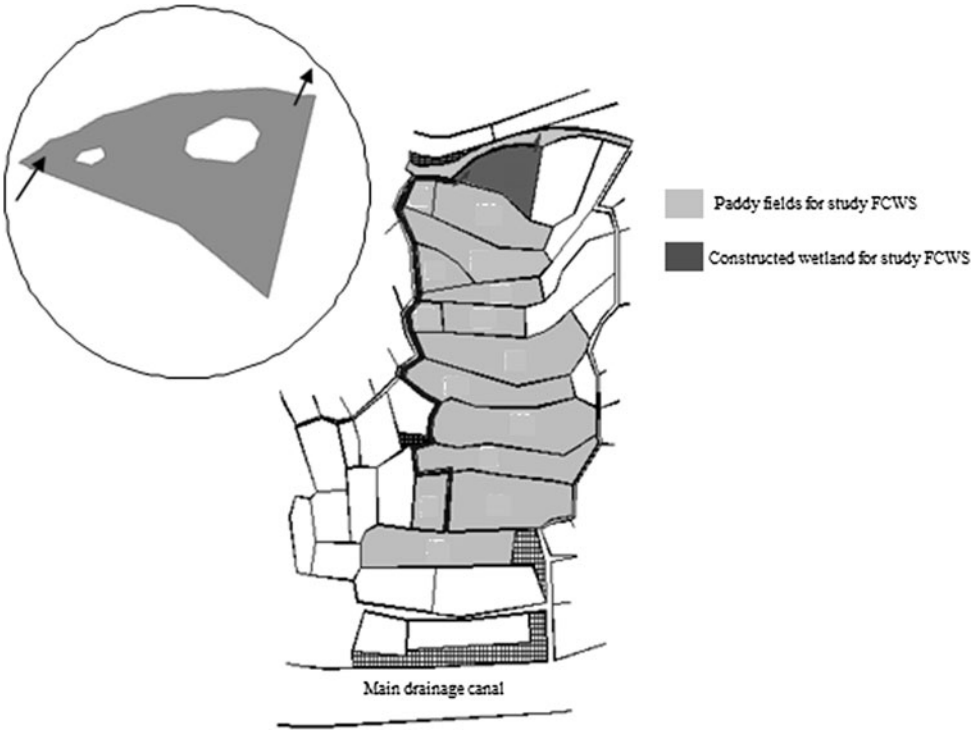

Fig. 3 Layout of paddy fields that drain to the Guilin FCWS

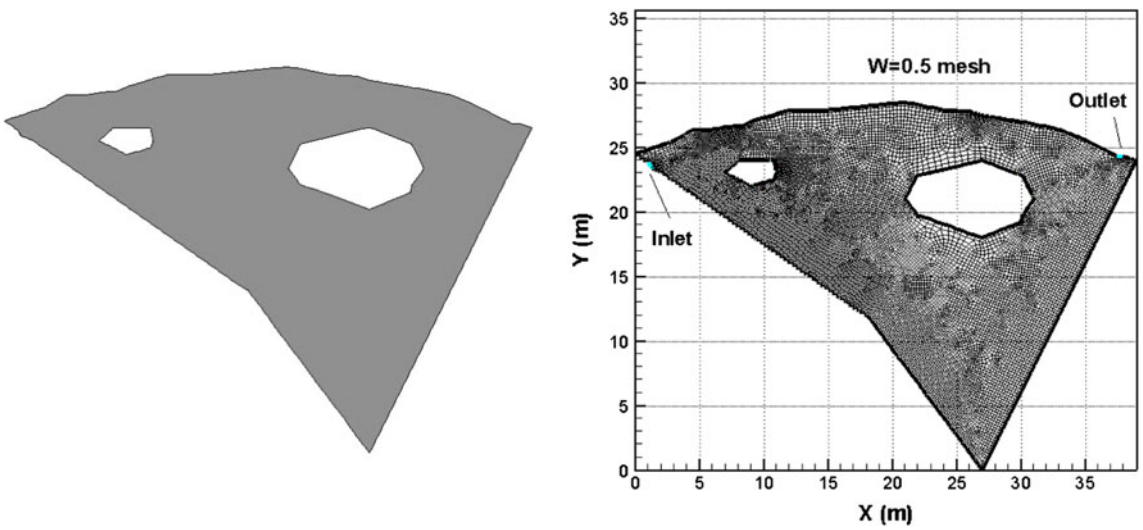

Fig. 4 The modeled two-dimensional mesh of the basin

2007). The wetland basin within the Cartesian coordinate system is illustrated in Fig. 4. The first part of this study which include nine case studies with distinct combinations of inlet width (0.5, 0.7 and 1.0 m) and mass inflow rate (2, 20 and 200 l/s). The second part of this study includes the first 9 case studies as well as 27 different cases with distinct combinations of inlet width (0.5–1.0 m) and mass inflow rate (200–1,200 l/s). These study parameters included extreme flow conditions that might be observed in this basin. The mass flow rate of 2 l/s represents the minimal rate recorded at the basin by the Guilin Experiment Station staff. Assumption for the modeling include negligible evaporation or evapotranspiration losses, a zero graded wetland bottom, homogenous vegetation providing a constant roughness coefficient (0.03), negligible wetland porosity such that mass exchanges between the surface and subsurface water are negligible (Bolster and Saiers 2002; Chow 1959).

The hydrodynamic flow field of each of the 36 cases is solved producing numerical flow variable values. Then these values are used as input for the development of stochastic multivariate models to predict turbulent dissipation characteristics and dynamic pressure variations within the basin. Wei et al. (2009) conducted preliminary studies of a set of 27 numerical cases provide better interpretation of the influence of extreme flow conditions. Wei et al. analyzed different combinations of mass inflow rate and inlet geometry, including inlet width ranging between 0.5 and 1.0 m, and mass inflow rate ranging from 2 to 1,200 l/s.

2 Mathematical model applications and analysis

2.1 Numerical formulations

2.1.1 Governing equations

The flow dynamics within the wetland basin are simulated using Conservation of Mass and Navier–Stokes equations with Reynolds Averaging (NSRA). The $k \sim \omega$ model is used to simulate flow (Menter 1994). This model is a two-equation, eddy-viscosity model, which is used as a low-Reynolds number turbulence model without any extra damping functions. The $k \sim \omega$ model integrates the viscous sub-layer flow, and performs well in cases with adverse pressure gradients (Umlauf et al. 2003). The governing equations for incompressible flow that are included in Fluent™ (Fluent 6.3 2006) are:

Conservation of mass equation:

$$\frac{\partial v_x}{\partial x} + \frac{\partial v_y}{\partial y} = 0 \tag{1}$$

Momentum equations:

$$\rho\left(\frac{\partial v_x}{\partial t} + u\frac{\partial v_x}{\partial x} + v\frac{\partial v_x}{\partial y}\right) = \mu\left(\frac{\partial^2 v_x}{\partial x^2} + \frac{\partial^2 v_x}{\partial y^2}\right) - \frac{\partial p}{\partial x} + \rho g_x \tag{2}$$

$$\rho\left(\frac{\partial v_y}{\partial t} + u\frac{\partial v_y}{\partial x} + v\frac{\partial v_y}{\partial y}\right) = \mu\left(\frac{\partial^2 v_y}{\partial x^2} + \frac{\partial^2 v_y}{\partial y^2}\right) - \frac{\partial p}{\partial y} + \rho g_y \tag{3}$$

Kinematic eddy viscosity equation:

$$v_T = \frac{a_1' k}{\max\left(a_1'\omega, S' F_2\right)}$$

Turbulence kinetic energy represented as k-equation:

$$\frac{\partial k}{\partial t} + v_x\frac{\partial k}{\partial x} + v_y\frac{\partial k}{\partial y} = p_k - \beta^* k\omega + \frac{\partial}{\partial x}\left[\left(v_y + \sigma_k v_T\right)\frac{\partial k}{\partial x}\right] + \frac{\partial}{\partial y}\left[\left(v_y + \sigma_k v_T\right)\frac{\partial k}{\partial y}\right] \tag{4}$$

Specific dissipation rate represented as ω-equation:

$$\frac{\partial \omega}{\partial t} + v_x\frac{\partial \omega}{\partial x} + v_y\frac{\partial \omega}{\partial y} = \alpha S'^2 - \beta\omega^2 + \frac{\partial}{\partial x}\left[\left(v + \sigma_\omega' v_T\right)\frac{\partial \omega}{\partial x}\right] + \frac{\partial}{\partial y}\left[\left(v + \sigma_\omega' v_T\right)\frac{\partial \omega}{\partial y}\right] + 2(1 - F_1)\sigma_{\omega^2}'\frac{1}{\omega}\left(\frac{\partial k}{\partial x}\frac{\partial \omega}{\partial x} + \frac{\partial k}{\partial y}\frac{\partial \omega}{\partial y}\right) \tag{5}$$

where the Reynolds number for turbulent flow is defined as $R_{eT} = \frac{k}{\omega v}$.

Closure coefficients and auxiliary relationships are as follows (Fluent 6.3 2006):

$$F_2 = \tanh\left\{\left[\max\left(\frac{2\sqrt{k}}{\beta^*\omega y}, \frac{500v}{y^2\omega}\right)\right]^2\right\} \tag{6}$$

$$p_k = \min\left(\tau\frac{\partial u_i}{\partial x_j}, 10\beta^* k\omega\right) \tag{7}$$

$$F_1 = \tanh\left\{\left\{\min\left[\max\left(\frac{\sqrt{k}}{\beta^*\omega y}, \frac{500v}{y^2\omega}\right), \frac{4\sigma_{\omega_2}' k}{CD_{k\omega} y^2}\right]\right\}^4\right\} \tag{8}$$

$$CD_{k\omega} = \max\left(2\rho\sigma_{\omega_2}'\frac{1}{\omega}\frac{\partial k}{\partial x_i}\frac{\partial \omega}{\partial x_i}, 10^{-10}\right) \tag{9}$$

$$\phi = \phi_1 F_1 + \phi_2(1 - F_1) \tag{10}$$

The model constants contained in the above closure and auxiliary relationships are:

$$\alpha_1 = \frac{5}{9},\ \alpha_2 = 0.44,\ \beta_1 = \frac{3}{40},\ \beta_2 = 0.0828,\ \beta^* = \frac{9}{100}$$

The model constants in Eqs. 6–10 are:

$$\sigma'^{*} = \frac{1}{2},\ \sigma'_{k_1} = 0.85,\ \sigma'_{k_2} = 1,\ \sigma'_{\omega_1} = 0.5,\ \sigma'_{\omega_2} = 0.856.$$

2.1.2 Other details of simulation process

Governing equations were solved using Fluent™. The flow domain of the wetland basin was divided into small finite volume cells as shown in Fig. 4 with a structural tetragonal mesh. The governing NSRA process with k and ω equations were integrated over each cell to generate a linear system of equations. These were solved systematically for each cell in the flow domain.

Convective and diffusive fluxes were calculated using the second-order upwind and central differencing scheme. These linear equations were iteratively solved until convergence when the residuals were sufficiently small for each equation. A time-marching procedure with first order accurate forward differencing time integration was applied to reach steady-state solutions until the variation of each parameter between two successive steps was insignificant over the domain.

Water density and viscosity was specified to be 1,000 and 0.001 kg/m^3, respectively, for the numerical simulations. Temperature was assumed to be 25°C. The walls of the basin mesh in Fig. 4 were applied with a no-slip condition. The initial wall roughness height was taken from Chow (1959) to be 0.005 m and the roughness constant to be 0.03 for the vegetative basins. The following provides simulation results for the hydrodynamic parameters velocity, dynamic pressure, viscous drag, and wall shear stress.

2.2 Results and discussion

2.2.1 Velocity

Figure 5 illustrates modeling results for all combinations of mass inflow rate (2, 20 and 200 l/s) with inlet width (0.5, 0.7 and 1.0 m), and provides insight into the phenomenon of short-circuiting and dead zones within the basin. For a given width, say 0.5 m, as mass flow rate increases, the potential for dead zones is reduced, and the potential for short-circuiting increases. These results are related to the spatial influence of the location of the inlet and the small island, as well the location of the larger island. Initially the small island helps dissipate some of the flow energy and distributes the inflow in two directions. The second island continues to influence short-circuiting. Short-circuiting needs to be minimized so that a design residence time is maintained for proper treatment. Velocity magnitude illustrated in Fig. 5 changes with the change in inflow rate and inlet width.

Flow velocity values are dimensionally small, i.e., ranging from 0.00005 to 0.0030 m/s, in the above simulation results. Therefore, the simulation results presented below are based on the maximum velocity for each of 27 inlet width and inflow rate combinations. For the following section we are evaluating the simulation results for inflow rates in the range of 2–1,200 l/s with the range of inlet widths from 0.5 to 1.0 m. These results are illustrated in Fig. 6. As expected there is a linear increase in velocity with increasing inflow rate, and maximum velocity, $E(v)$, decreases as inlet width increases in the order:

$$E(v)_{0.5} > E(v)_{0.6} > E(v)_{0.7} > E(v)_{0.8} > E(v)_{0.9} > E(v)_{1.0}$$

2.2.2 Dynamic pressure

Dynamic pressure is similar to the kinetic energy of a fluid particle and is the pressure due to the passage of water through the wetland. Figure 7 illustrates maximum dynamic pressure variation as a function of inflow rate. Peak dynamic pressure within the wetland basin increases with increased inflow rate. Maximum dynamic pressure, $E(p)$, varies with width in the following order:

$$E(p)_{0.5} > E(p)_{0.6} > E(p)_{0.7} > E(p)_{0.8} > E(p)_{0.9} > E(p)_{1.0}$$

The maximum pressure distribution (Fig. 7) illustrates the characteristics of Stokes flow (Keller 2003), where the peak dynamic pressure within the basin follows a linear trend with inlet width in the range of 0.9–1.0 m. Peak dynamic pressure in the basin with inlet widths less than 0.9 m is nonlinear.

2.2.3 Dissipation rate

A properly designed wetland basin should reduce the energy consumption required to minimize turbulent dissipation. The specific dissipation rate, ω, is the rate of dissipation of turbulence per unit of energy. Dissipation rate varies with increase in inflow rate. In general, peak dissipation rate $E(\omega)$ varies with inlet width as:

$$E(\omega)_{0.6} > E(\omega)_{0.7} > E(\omega)_{0.8} > E(\omega)_{0.5} > E(\omega)_{1.0} > E(\omega)_{0.9}$$

The random behavior of increasing ω as a function of inflow rate is illustrated in Fig. 8 with respect to inlet width. Figure 8 also illustrates a width-specific effect on the variation of maximum dissipation rate within the basin. Compared to the case with inlet widths of 0.5, 0.9 and 1 m, the case with inlet widths of 0.6, 0.7 and 0.8 m would provide better dissipation features.

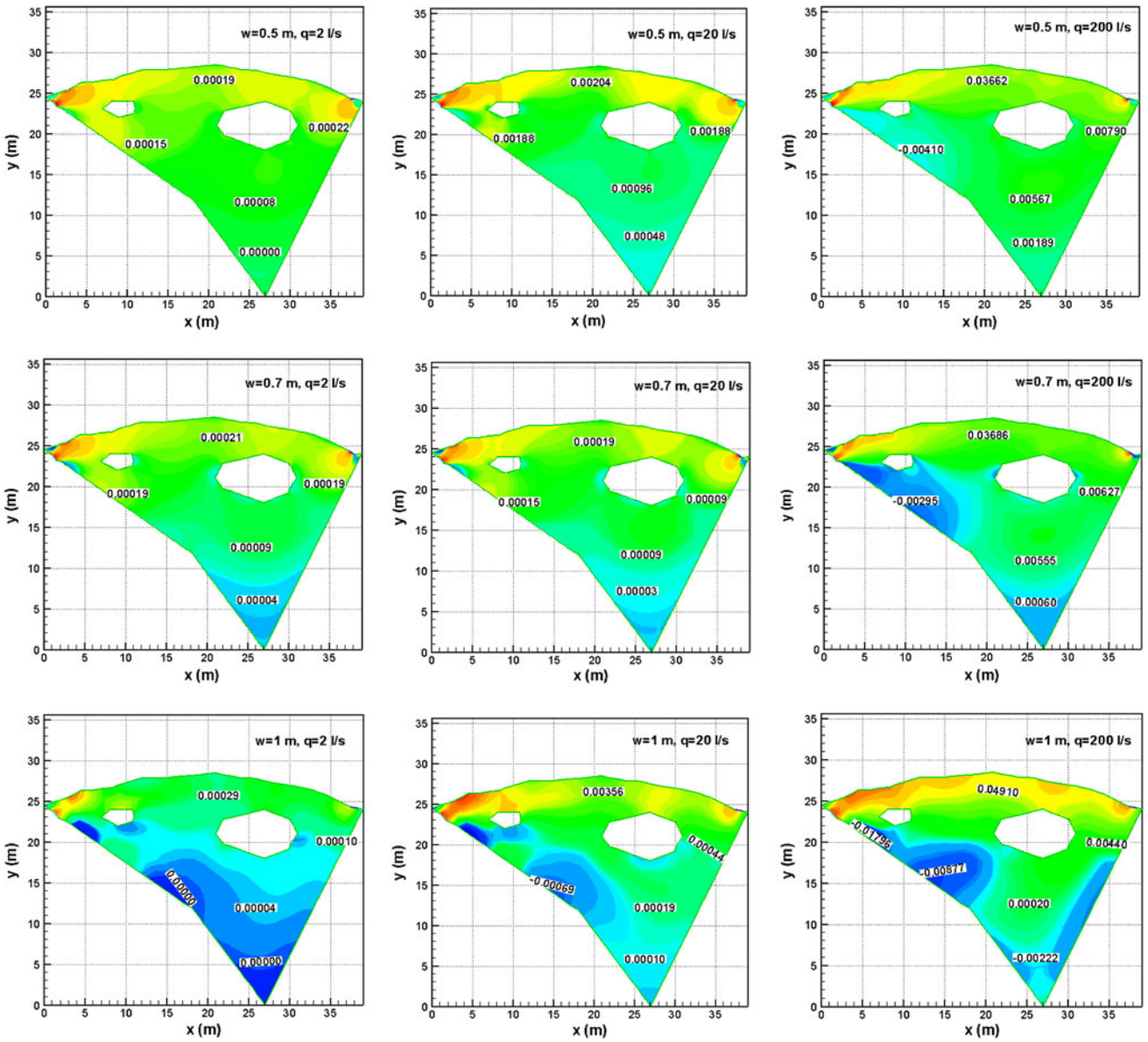

Fig. 5 Comparison of velocity contours with change in inlet width (0.5, 0.7 and 1.0 m) and inflow rate (2, 20 and 200 l/s)

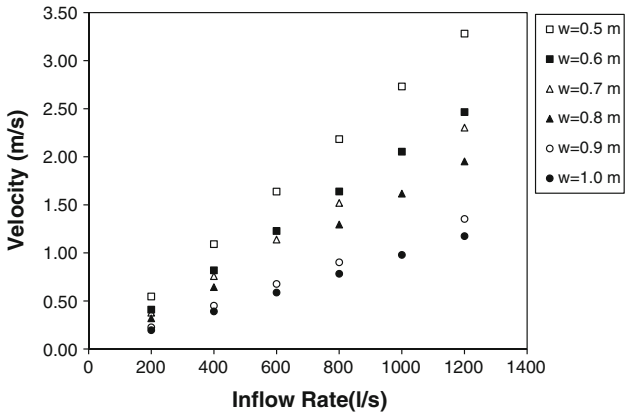

Fig. 6 Maximum velocity as a function of inlet width and inflow rate

2.2.4 *Wall shear stress*

From Fig. 9, wall shear stress, τ, is directly proportional to the inflow rate. Wall shear stress plays a role in predicting dissipation rates along the basin wall, but dissipation rates are negligible away from the basin walls (Jovanovic et al. 1995). Maximum wall shear stress, $E(\tau)$, varies with width in the order:

$$E(\tau)_{0.8} > E(\tau)_{0.6} > E(\tau)_{0.7} > E(\tau)_{0.9} > E(\tau)_{0.5} > E(\tau)_{1.0}$$

The wetlands with inlet width of 0.6, 0.7 and 0.8 m respectively tend to have similar wall shear stresses within the respective wetlands.

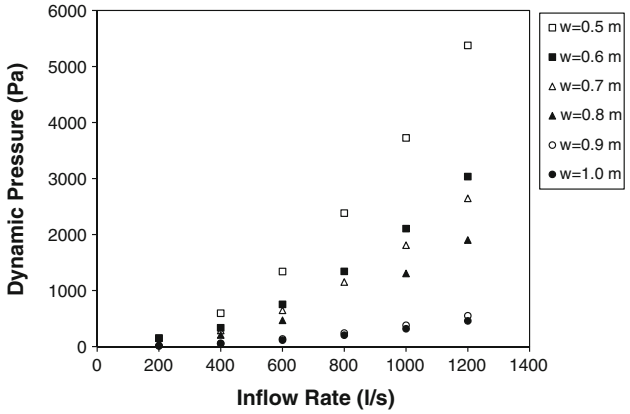

Fig. 7 Maximum dynamic pressure for changes in inlet width and inflow rate

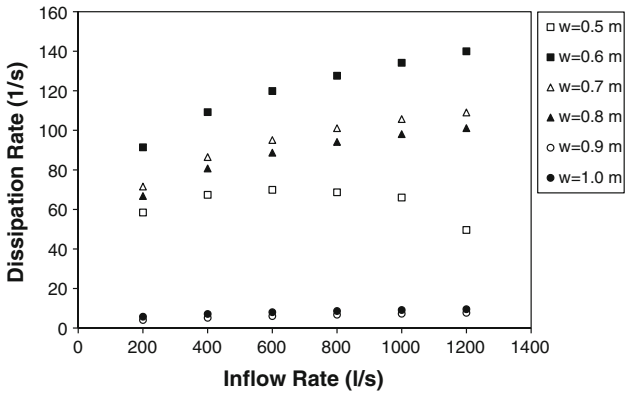

Fig. 8 Change in maximum dissipation rate, ω, with change in inlet width and inflow rate

3 Stochastic multi-parameter model application and comparison

3.1 Theoretical framework

Stochastic methods have been widely used in the fields of hydrology (Cantet et al. 2011; Haan 1994; Lee and Yoo 2001), hydraulics (Chen et al. 2009; Erik 2011; Kim et al. 2004) and agriculture (Perreault et al. 2000; Wu and Wang 1998; Young et al. 2011). The nonlinear nature of dynamic pressure and dissipation rate is confirmed from Figs. 7 and 8, and a multiplicative or lognormal model may be representative of the variability of these variables' relationship (Benjamin and Cornell 1970). The management and construction of treatment wetlands relies on a quantitative understanding of surface water flows as a function of geometrical and flow aspects as well as the resistance offered by the vegetation within the wetland. Therefore, assume the response variable, Y_i, represents the variation in dynamic pressure, as well as dissipation rate, each of which is a function of the predictor variable, X_i, expressing inlet

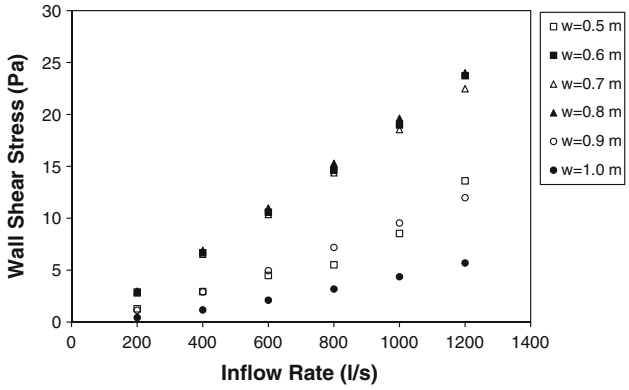

Fig. 9 Maximum wall shear stress changes corresponding to changes of inlet width and inflow rate

width, W, inflow rate, q, and possibly other predictor variables, the nonlinear model can be expressed as:

$$\frac{Y_i}{Y_{i-1}} = X_i^{b_i}, \quad \text{for } i = 1, 2, \ldots, k \tag{11}$$

where the Y_i are response variables, the X_i are predictor variable, and b_i are model constants (Soboyejo and Nestor 2000).

Equation 11 is a stochastic nonlinear model, showing the relationship between the flow characteristic Y_i at step i and its value at step $i-1$. In Eq. 11 the transfer function $X_i^{b_i}$ contains the effect of the predictor variable X_i at step i (Benjamin and Cornell 1970). Since there are k predictor variables in the generalized multi-parameter stochastic model, Eq. 11 represents only one of the steps for $i = 1, 2, \ldots, k$. Equation 11 is extended to a multi-parameter multiplicative model to predict nonlinear flow characteristics on the basis of inflow rate, $q = X_1$, and width specific parameter, X_2, and other predictor parameters,

$$Y_i = Y_0 X_1^{b_1} X_2^{b_2} \ldots X_k^{b_k}$$

Let the initial value of Y_0 represented by an alphabet a for simplicity, then

$$Y_i = a \prod_{i=1}^{k} X_i^{b_i} \tag{12}$$

Let $y = y_i = \ln Y_i$, Eq. 12 can be linearized as shown in Eq. 13,

$$y = \ln a + \sum_{i=1}^{k} b_i \ln X_i \tag{13}$$

The predictor parameters X_i in Eqs. 12 and 13 are dimensionally distinct and can be represented using different units, Eq. 12 is reformulated to provide dimensional similarity. This is performed as (Soboyejo and Nestor 2000):

$$Y/Y_0 = \prod_{i=1}^{k} (X_i/X_{i0})^{b_i} \quad (14)$$

where X_{i0} is the maximum constant value to the predictor variable X_i for $i = 1, 2,\ldots, k$ and has the same physical unit as X_i. Both the left and right sides of Eq. 14 are dimensionless. The model constant a can be represented by Soboyejo and Nestor (2000):

$$a = Y_0 \left\{ \prod_{i=1}^{k} X_{i0}^{b_i} \right\}^{-1} \quad (15)$$

3.2 Discussion and multi-parameter development

3.2.1 *Case I: dynamic pressure variation and prediction models*

The known parameters of inlet width, W, and inflow rate, q, are used as inputs to the two-dimensional flow model. The results of the flow modeling were plotted in Figs. 5, 6, 7, 8, 9. From Fig. 7, dynamic pressure variation was found to be nonlinear with inflow rate and inlet width of the wetland. Hence, dynamic pressure, p, is written as:

$$p_i = a \prod_i X_i^{b_i} \quad \text{for } i = 1, 2, \ldots, n \quad (16)$$

Equation 16 is a stochastic model showing the relationship between p_i at step i from the dynamic pressure at step $i - 1$ and transfer function $X_i^{b_i}$. This transfer function $X_i^{b_i}$ lumps in the effect of the inflow rate, X_i, for $i = 1$ for any specific inlet width under consideration.

Table 1 represents the results of regression analysis and values for the model constants a and b_1. It also gives the Coefficient of Determination, R^2, and the Sample Standard Deviation, S. The R^2 values are encouraging.

When considering the flow in the wetland basin, the wetland's shape and inflow rate have great influence on flow behavior (Persson et al. 1999). In order to further study the influence of inflow rate and inlet width parameters, Eq. 16 is transformed as shown below to include inlet width parameter, X_2, for inlet width, W. This parameter lumps the combined effects of inlet width and inflow rate influencing the variation in dynamic pressure within the basin (Soboyejo et al. 2001). Following the theoretical framework proposed for the derivation of Eq. 12, the dynamic pressure p within the wetland can be expressed as:

$$p = \overline{a} X_1^{\overline{b_1}} X_2^{\overline{b_2}} \quad (17)$$

where $\overline{a}$, $\overline{b_1}$ and $\overline{b_2}$ are model constants.

The results in Table 2 confirm the influence of inflow rate on dynamic pressure in the wetland basin. Theoretical models in Table 2 and experimental cumulative frequency of p are found to have a maximum discrepancy, $D_n = 0.084$. The maximum discrepancy, D_n, is found to be less than the critical maximum difference $D_n^{0.05} = 0.23$ (Ang and Tang 1984).

Therefore, the model proposed in Table 2 is appropriate at a 5% significance level for predicting p as illustrated in Table 3 below.

The theoretical multi-parameter model in Eq. 17 predicts peak dynamic pressure in the wetland basin with 99.8% accuracy as illustrated in Fig. 9. The model in Table 2 also satisfies

$$\mathrm{Var}(p) \approx \left(\overline{b_1}\right)^2 \mathrm{Var}(X_1) + \left(\overline{b_2}\right)^2 \mathrm{Var}(X_2) \quad (18)$$

where

$\mathrm{Var}(p) = 2.349 \approx (2.01)^2 \times 0.376 + (0.989)^2 \times 0.848.$

The mathematical verification of Eq. 18 also confirms the major influence of inflow rate on the dynamic pressure variation in the wetland basin. Figure 10 plots the dynamic pressure variations as simulated by the two dimensional numerical models as a function of dynamic pressure predicted from the stochastic model enumerated in Table 2.

Table 1 Model coefficients of determination and error in the model for p as a function of inflow rate $q = X_1$ following $p = f(X_1) = aX_1^{b_1}$

W	Model	a	b_1	R^2	S
0.5	$p_{(0.5)}$	−5.59	2.00	99.6	0.00181
0.6	$p_{(0.6)}$	−6.18	2.00	99.7	0.0026
0.7	$p_{(0.7)}$	−6.39	2.01	99.9	0.0062
0.8	$p_{(0.8)}$	−6.76	2.02	99.8	0.0035
0.9	$p_{(0.9)}$	−7.99	2.02	99.9	0.0029
1.0	$p_{(1.0)}$	−8.03	2.00	99.8	0.0002

$p_{(0.5)}$ stands for the dynamic pressure variable when inlet width is 0.5 m; similar for $p_{(0.6)}$–$p_{(1.0)}$

Table 2 Stochastic model for p as a function of inflow rate $q = X_1$ and inlet width $W = X_2$ following Eq. 17 as $p = f(X_1, X_2)$

Predictor variables	$\overline{a}$	$\overline{b_1}$	$\overline{b_2}$	S	R^2
X_1	−6.82	2.01	0	0.92	64.6
X_2	−0.075	2.01	0.989	0.06	99.92

Table 3 D_n and $D_n^{0.01}$ of Kolmogorov–Smirnov test for evaluating the model in Table 2

Kolmogorov–Smirnov test at 5% level of confidence			
Model	D_n	Number of data samples	Critical value of $D_n^{0.05}$
p	0.084	36	0.23

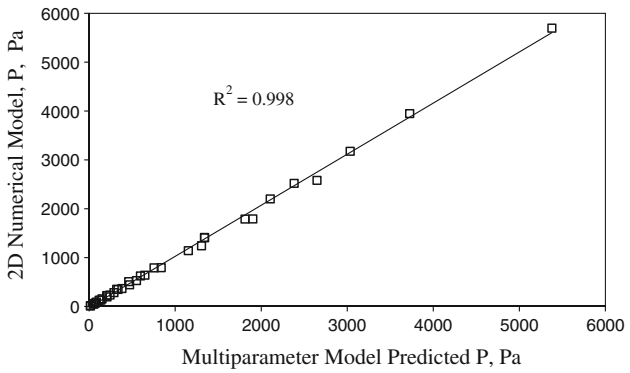

Fig. 10 Peak dynamic pressures from numerical models as a function of stochastic prediction of dynamic pressure by Eq. 17

The accuracy of the stochastic models is confirmed since the two-dimensional numerical simulation results match the results from the stochastic multi-parameter model.

3.2.2 *Case II: dissipation as a function of inlet width factor, q, and wall shear stress*

Figure 9 illustrates a unique characteristic of wall shear stress to increase irrespective to the variations of flow rate, X_1, at their corresponding inlet geometry of the wetland basin. Figure 8 illustrates the random behavior of the specific dissipation rate irrespective of the flow rate, X_1, and corresponding inlet geometry parameter, X_2. The actual behavior of these parameters including inflow rate, X_1, geometrical parameter, X_2, and wall shear stress, X_3, is hidden but mathematically correlated. The inclusion of the geometrical parameter is important to assess the timely variation of the boundaries of the wetland with flooding and drought events (Feng and Molz 1997). This will help to also assess the need for structural changes in wetland design (Swain 1999).

The observed nonlinear development of specific dissipation rate, $\omega = D_i$, as visually depicted in Fig. 7 is written in lognormal form as shown below in Eq. 19:

$$D_i = D_0 X_1^{c_1} X_2^{c_2} \ldots X_k^{c_k} = f \prod_{i=1}^{k} X_i^{c_i} \tag{19}$$

where f, D_0 and c_1, c_2,…,c_k are model constants specific to the wetland basin geometry under study and dependent on the predictor variables discussed.

$$d = d_i = \ln D_i = \ln f + \sum_{i=1}^{k} c_i \ln X_i \tag{20}$$

The log-transformation (Eq. 20) reduces the magnitude of the experimental data, thus reducing the magnitude of the mean and error values associated with these data. Equation 19 therefore, represents an autonomous equation, D, which is differentiable in its present form. The initial value of f changes with each new function of X_i for $i = 1, 2,\ldots, k$. These functions introduce new relationships between the response variable, D, and each random variable, X_i, for $i = 1, 2,\ldots, k$ (Tabuada and Pappas 2005).

The dissipation rate function, D_i, is to be modeled to better predict the boundary conditions of the free water surface and wall-bounded shear flows in constructed basins. Therefore, it is desirable to develop a new single quantity which is an observable random variable that can predict the stochastic development of these properties. The observable new quantity should be a simpler representation of the response variable, $D_i = Y_i$ (dissipation rate function), while preserving its trends and original properties. In order to develop this, the construction of a quotient variable is proposed as:

$$G = G_i = X_1/D_i \tag{21}$$

where X_1 is inflow rate (Sussman 1977). The authors note that the variable X_1 is the most influential input parameter in this study. The random variable G_i jointly characterizes random variables X_1 and D_i (Pappas and Simic 2002).

The new random variable G_i maps subjective to $Y_i(=D_i)$ as shown in Fig. 11, which confirms that G_i inherited the mathematical properties of Y_i. This implicitly indicates that input predictor variables of original response variable Y_i become inputs of G_i as illustrated in Eq. 21.

It is to be noted that Y_i in the figure is the dissipation rates (D_i or ω) derived from the two dimensional numerical simulation. Then, following Eq. 11, the stochastic development of G_i can be written as:

$$G_1/G_0 = X_1^{c_1} \tag{22}$$

The transfer function $X_1^{c_1}$ represents the effects of inflow rate, X_1, for each corresponding inlet width. Table 4 presents the results of regression analysis which gives values for the model constants f and c_1, as well as model R^2 and S values. Again, the R^2 values are encouraging.

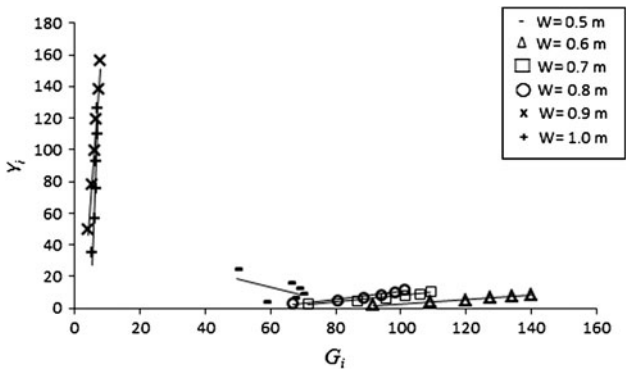

Fig. 11 Original variable Y_i versus quotient response variable G_i

Table 4 Model constants, coefficients of determination and error of model for G as a function of inflow rate $q = X_1$ following $G_1 = f\prod_{i=1} X_1^{c_1}$

W	Model	f	c_1	R^2	S
0.5	$G_{0.5}$	−4.32	1.03	96.4	0.146
0.6	$G_{0.6}$	−3.27	0.764	100	0.0060
0.7	$G_{0.7}$	−3.04	0.765	99.9	0.013
0.8	$G_{0.8}$	−2.99	0.768	99.9	0.015
0.9	$G_{0.9}$	0.510	0.640	100	0.0063
1.0	$G_{1.0}$	−0.249	0.716	100	0.0107

When considering how flow is modified within wetland basins, wall-bounded flow should minimize viscous drag (Frohnapfel et al. 2007). The relationship between inlet geometry and inflow rate provides information for determining the maximum pressure differences within the basin as shown in Eq. 17. These pressure differences are basically caused by the friction drag applied by the basin walls.

The new model constant $\overline{f}$ in Eq. 23 combines the effects of changes of inflow rate, X_1, basin geometry, X_2, and wall shear stress, X_3 which influence the variation of dissipation rate, ω, within the basin. From the theoretical framework proposed for deriving Eq. 12 the new variable G can be expressed as:

$$G = f(X_1, X_2, X_3) = \overline{f} X_1^{\overline{c_1}} X_2^{\overline{c_2}} X_3^{\overline{c_3}} \tag{23}$$

Further explanation of the framework followed in Eq. 23 is found elsewhere and interested readers are requested to refer Soboyejo et al. (2001). Equation 23 can now be linearized and expressed as:

$$g = g_i = \ln G = \ln \overline{f} + \sum_{i=1}^{3} \overline{c}_i \ln X_i \tag{24}$$

where c_1, c_2 and c_3 are the model constants. Now the independent variables X_1, X_2 and X_3 are pooled as per requirements for Eq. 23 as shown above.

The predictor variables of Eq. 23 are outputs of the flow modeling studies enumerated earlier with Figs. 3 and 4. These predictor variables are interdependent and have a correlation coefficient $\rho_{x_{i,j}}$. Values of $\rho_{x_{i,j}}$ between these variables X_i arranged in i rows and j columns are represented in the matrix form as $\rho_{x_{i,j}}$ in Table 5, where $i = 0, 1, 2,\ldots, n$ and $j = 0, 1, 2,\ldots, k$.

Mathematically, correlation $\rho_{x_{i,j}}$ between the predictor variables $X_{x_{i,j}}$ enumerated in Table 5 can be linearly mapped onto independent predictor variables $V_i = \overline{V_{i,j}}$ and scaled using Eq. 25:

$$\frac{\left(\left[X_{i,j} - \mu x_{i,j}\right]\right)}{\sigma x_{i,j}} = [\overline{T}]\left[\frac{[\overline{v_{i,j}}]}{\sqrt{\lambda_{i,j}}}\right] \tag{25}$$

Table 5 Correlation coefficient $\rho_{x_{i,j}}$ between predictor variables of Eq. 23

Predictor variables	X_1	X_2	X_3
X_1	1	0	0.78
X_2	0	1	−0.358
X_3	0.78	−0.358	1

where $\mu_{x_{i,j}}$ and $\sigma_{x_{i,j}}$ are the mean and standard deviation of the original interdependent variables $X_{i,j}$ for $i = 0, 1, 2,\ldots, n$, $j = 0, 1, 2,\ldots, k$ and $n > k$. The function $[\overline{T}] = [\Phi]^{\tau}$ represents the transpose of the null space $[\xi_{i,j}]$ in the normalized form (Plappally et al. 2010). The characteristic equation can be expressed as:

$$\left[\lambda_{i,j}[I] - \left(\rho_{X_{i,j}}\right)\right][\xi_{i,j}] = 0 \tag{26}$$

where $i = 0, 1, 2,\ldots, n$, $j = 0, 1, 2,\ldots, k$ and $n > k$. From Eq. 26, there will be one eigen space $[\xi_{i,j}]$ for each distinct eigenvalue $\lambda_{i,j}$. There will be k eigen spaces for $\left(\rho_{X_{i,j}}\right)$. The trace of the eigenvalue matrix $\left(\sum_{i=1}^{k}\lambda_{i,j}\right)$ also defines the total variance of the independent predictor variables V_i. Equation 26 may be rewritten in the form:

$$G = e^{f'} V_1^{vc_1} V_2^{vc_2} \ldots V_k^{vc_k} \tag{27}$$

where f', vc_1, vc_2, …, vc_k represent the constants of the new independent predictor variables $V_{i,j}$ for $i = 1, 2, 3, \ldots, k$. These constants indicate the importance and hierarchy of their influence, which is helpful in finding design value of the major predictor variable X_i influencing the original response variable Y.

Multivariate regression results from Table 5 can then be expressed as:

$$G = \mathrm{e}^{2.76} V_1^{-0.109} V_2^{-1.24} V_3^{-0.999} \tag{28}$$

Equation 28 illustrates the maximum influence of flow rate on the stochastic development of G with a $R^2 = 96.2$, and a standard error of 0.271. Now, the variance of the parameters in Eq. 28 can be described as:

$$\mathrm{Var}(g) \approx (vc_1)^2 \mathrm{Var}(V_1) + (vc_2)^2 \mathrm{Var}(V_2) + (vc_3)^2 \mathrm{Var}(V_3) \tag{29}$$

where $\mathrm{Var}(g) = 1.77 \approx (-0.109)^2 \times 1.858 + (-1.24)^2 \times 1 + (-0.999)^2 \times 0.1416$. The mathematical verification of Eq. 29 confirms the major influence of inlet geometry on G. The theoretical model in Eq. 28 and the experimental cumulative frequency of G are found to have a maximum discrepancy $D_n = 0.197$ at a p^- value $p < 0.01$. The maximum discrepancy D_n is found to be less than critical maximum difference $D_n^{0.05} = 0.23$ (Ang and Tang 1984). Therefore the

model proposed in Eq. 28 is appropriate at the 5% significance level for predicting G, as illustrated in Table 6 and in Fig. 12.

4 Implications

Since complex mathematical models available for predicting surface water flow characteristics through wetlands cannot be easily applied by lay technicians, the simple multi-parameter modeling approach is developed in this article. Design requirement of dynamic pressure can be easily predicted for any specific riparian wetland with a known inflow rate and geometry by similar multi-parameter models as depicted in Table 2. A negative correlation is found between the variables of inlet geometry and variation of shear stress within the wetland. This implies that a dimensional variation of the wetland would have a greater effect on the flow resistance.

Wetland specific dissipation rate can be controlled with small changes in the geometry of the wetland basin, particularly the inlet width. Inflow rate is a major player in managing dissipation rate, since with changes in geometry, inflow rate will change. Both parameters discussed tend to positively affect each other. The control of viscous dissipation can be used to improve the residence time within the wetland basin for particles and solutes, thus the treatment characteristics of the design of the constructed wetland can help to improve water quality.

5 Summary and conclusions

The combination of $k \sim \omega$ model as well as stochastic regression provides a very efficient tool to provide deep understanding of flow characteristics while designing constructed wetlands. The $k \sim \omega$ flow model simulation results for wetland hydrodynamics are correlated with each other. This hides the independent influences of parameters impacting flow characteristics. A subroutine inclusive of information in Table 5, Eqs. 23 and 24 is to be appended to the $k \sim \omega$ flow model simulation post processing program to remove correlation between its output results. A summary of the results is given as shown below:

Table 6 D_n and $D_n^{0.05}$ of Kolmogorov–Smirnov test for evaluating the model in Eq. 27

Kolmogorov–Smirnov test at 5% level of confidence			
Model	D_n	Number of data samples	Critical value of $D_n^{0.05}$
g	0.197	36	0.23

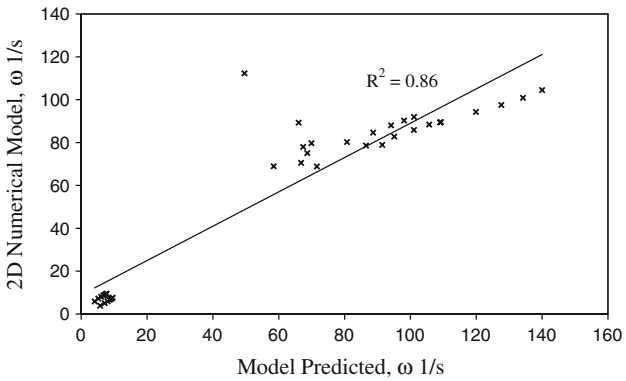

Fig. 12 Specific dissipation rate output of two dimensional numerical simulations as a function of stochastic model prediction in Eq. 26

(1) From the two-dimensional flow models, a size effect is clearly found to control the flow characteristics. The variation in inlet size has highly affected the flow characteristics. A change in the inlet width changes the dimension of wall perimeter in contact with surface water.
(2) The two-dimensional flow models clearly enumerate the decrease in the peak velocity magnitude within the wetland flow domain with increasing inlet width.
(3) Multi-parameter probabilistic modeling of Guilin constructed wetland variables has helped to combine interaction existing between the flow parameters as well as geometric variables at a shallow depth condition for the prediction of dynamic pressure and degree of turbulence dissipation.
(4) The dimensional features of the constructed wetland play an important role to improve the efficacy of the wetland in controlling viscous dissipation. A minor change in the wall perimeter of the wetland can effect changes in dissipation rates.
(5) The models clearly enumerate the dependence of inlet size and inflow rate in the development of dynamic pressure and dissipation rates. Inflow rate is the major variable influencing the dynamic pressure within a wetland system.
(6) Simplified multi-parameter stochastic quotient based lognormal model is proposed to predict the peak measure of turbulence dissipation in constructed wetlands. The simple stochastic models developed are capable of predicting peak dynamic pressure variation and specific dissipation rate with high accuracy for free and wall bounded surface flows through constructed wetlands.

Acknowledgments The authors wish to acknowledge the support received from the Guilin Center Station of Irrigation and Drainage, China. The project *Farmland nonpoint pollution control technique*

experiment research and demonstration funding was provided by the Ministry of Water Resources of China and the International Program for Water Management in Agriculture at The Ohio State University.

References

Allred B, Fausey N, Brown L (2001) Wetland Reservoir Subirrigation Systems (WRSIS). USDA-ARS, Columbus, Ohio. http://www.ars.usda.gov/Main/docs.htm?docid=14999&pf=1&cg_id=0. Accessed January 2011

Allred B, Brown L, Fausey N et al (2003) Water table management to enhance crop yields in a wetland reservoir subirrigation system. Appl Eng Agric Am Soc Agric Eng 19(4):407–421

Allred B, Fausey N, Brown L, et al (2007) Wetland Reservoir Subirrigation System (WRSIS). USDA-ARS, Columbus, Ohio. http://www.ars.usda.gov/Research/docs.htm?docid=14999. Accessed March 2011

Ang A, Tang W (1984) Probability concepts in engineering planning and design. Volume II—decision, risk and reliability. Wiley, New York

Benjamin J, Cornell A (1970) Probability statistics and decisions for Civil Engineers. McGraw Hill Book Company, New York

Bernhard H, Michael A, Ursula S (2004) Salt tracer experiments in constructed wetland ponds with emergent vegetation: laboratory study on the formation of density layers and its influence on breakthrough curve analysis. Water Res 38:2095–2102

Bolster C, Saiers J (2002) Development and evaluation of a mathematical model for surface-water flow within the Shark River Slough of the Florida Everglades. J Hydrol 259(1–4):221–235

Cantet P, Bacro J, Arnaud P (2011) Using a rainfall stochastic generator to detect trends in extreme rainfall. Stoch Environ Res Risk Assess 25(3):429–441

Chen M, Keller A, Lu Z (2009) Stochastic analysis of transient three-phase flow in heterogeneous porous media. Stoch Environ Res Risk Assess 23(1):93–109

Chow V (1959) Open channel hydraulics, Chapter 5. McGraw-Hill Book Company, New York

Davies I, Hassan O, Jacob N, et al (2003) Probabilistic methods in fluids. Proceeding of The Swansea 2002 Workshop, World Sceintific Co. Pte. Ltd, Singapore

Erik V (2011) Long-term time-dependent stochastic modeling of extreme waves. Stoch Environ Res Risk Assess 25(2):185–209

Feng K, Molz FJ (1997) A 2-D diffusion-based, wetland flow model. J Hydrol 196(1–4):230–250

Fluent 6.3 (2006) Manual Fluent Inc (from the Ohio State University)

Frohnapfel B, Jovanovic J, Delgado A (2007) Experimental investigations of turbulent drag reduction by surface-embedded grooves. J Fluid Mech 590:107–116

Haan C (1994) Statistical methods in hydrology. Iowa State University Press, Ames

Jovanovic J, Ye Q, Durst F (1995) Statistical interpretation of the turbulent dissipation rate in wall-bounded flows. J Fluid Mech 293:321–347

Kadlec R (1999) Chemical, physical and biological cycles in treatment wetlands. Water Sci Technol 40(3):37–44

Keller J (2003) Minimum dissipation rate flow with given flux. J Fluid Mech 480:61–63

Kim B, Kim H, Seoh B (2004) Stream flow simulation and skewness preservation based on the bootstrapped stochastic models. Stoch Environ Res Risk Assess 18(6):386–400

Knight R, Payne V, Borer R et al (2000) Constructed wetlands for livestock wastewater management. Ecol Eng 15(1):41–55

Lee J, Yoo C (2001) An analysis of mean transition time between flood and drought in the large river basin. Stoch Environ Res Risk Assess 15(5):341–356

Menter F (1994) Two-equation eddy-viscosity turbulence models for engineering applications. AIAA J 32:269–289

Mitsch W, Wise K (1998) Water quality, fate of metals, and predictive model validation of a constructed wetland treating acid mine drainage. Water Res 32(6):1888–1900

Pappas G, Simic S (2002) Consistent abstractions of affine control systems. IEEE Trans Autom Control 47(5):745–756

Perreault L, Parent E, Bernier J, Bobee B, Slivitzky M (2000) Retrospective multivariate Bayesian change-point analysis: a simultaneous single change in the mean of several hydrological sequences. Stoch Environ Res Risk Assess 14(4):0243–0261

Persson J, Somes N, Wong T (1999) Hydraulic efficiency of constructed wetlands and ponds. Water Sci Technol 40(3):291–300

Plappally A, Soboyejo A, Fausey N, Soboyejo W, Brown L (2010) Stochastic modeling of filtrate alkalinity in water filtration devices: transport through micro/nano porous clay based ceramic materials. J Nat Environ Sci 1(2):96–105

Pokorny J, Kvet J, Rejskova A, Brom J (2010) Wetlands as energy-dissipating systems. J Ind Microbiol Biotechnol 37:1299–1305

Shan Z, Dong B, Li X et al (2008) Preliminary study on the new way to deal with non-point source pollution in rice-based irrigation system. China Rural Water Hydropower 3:62–65 (in Chinese)

Soboyejo A, Nestor K (2000) A new statistical biomechanics approach to modeling of bone strength in broiler chickens and turkeys. Part I—theoretical development; Part II—validation of theoretical models. Trans Am Soc Agric Eng 43(6):1997–2006

Soboyejo ABO, Ozkan HE, Papritan JC, Soboyejo WO (2001) A new multiparameter approach to the prediction of wear rates in agricultural sprayer nozzles. J Test Eval 29(4):372–379

Somes N, Bishop W, Wong T (1999) Numerical simulation of wetland hydrodynamics. Environ Int 25(617):773–779

Sussman H (1977) Existence and uniqueness of minimal realization of nonlinear systems. Math Syst Theory 10:263–284

Swain E (1999) Numerical Representation of dynamic flow and transport at the Everglades/Florida bay interface. 3rd International symposium on ecohydraulics, Salt Lake City, Utah, July 1999

Tabuada P, Pappas G (2005) Quotients of fully nonlinear control systems. SIAM J Comput 43(5):1844–1866

Tecplot Inc. (2007) Tecplot 360 User's Manual (from the Ohio State University)

Umlauf L, Burchad H, Hutter L (2003) Extending the $k \sim \omega$ turbulence model towards oceanic application. Ocean Model 5:195–218

Wei X, Wang X, Shan Z et al (2007) Improved farmland irrigation and drainage systems. Chin J Irrig Drain 5:1–3 (in Chinese)

Wei X, Plappally A, Mao Z, Brown L (2009) Simulation analysis of flow hydraulics in constructed wetland basins. ASABE annual international meeting, Reno, Nevada, June 23. Paper No. 097461

Wu F, Wang C (1998) Higher-order approximation techniques for estimating stochastic parameter of a sediment transport model. Stoch Hydrol Hydraul 12(6):359–375

Young H, Lim B, Lee E, Choi Y (2011) The impact of the risk environment and energy prices to the budget of Korean households. Stoch Environ Res Risk Assess 25(3):323–330